Article

Discovery Medicine 2025; 37(202): 2539–2551
https://doi.org/10.24976/Discov.Med.202537202.213

Modulating STAT3 Signaling by Selective C5aR1 Inhibition: An *In Silico* Directed *In Vitro* Approach to Combat Diabetic Kidney Disease

Ayed A. Dera[1,*], Mesfer Al Shahrani[1]

[1]Department of Clinical Laboratory Sciences, College of Applied Medical Sciences, King Khalid University, 61421 Abha, Saudi Arabia
*Correspondence: ayedd@kku.edu.sa (Ayed A. Dera)
Submitted: 18 May 2025 Revised: 3 July 2025 Accepted: 9 July 2025 Published: 20 November 2025

Background: Diabetic Kidney Disease (DKD) is a leading cause of chronic kidney disease (CKD) and end-stage renal failure. The complement component 5a (C5a)-C5a Receptor 1 (C5aR1) signaling axis plays a critical role in these pathological processes by activating inflammatory pathways, including signal transducer and activator of transcription 3 (STAT3) signaling, exacerbating kidney injury. As the current treatments for DKD fail to address the underlying inflammatory and fibrotic processes, targeting the C5a-C5aR1 pathway may be a novel therapeutic approach.

Methods: High-throughput virtual screening (HTVS) was conducted to screen C5a-C5aR1 inhibition. Selected compounds were further validated through molecular dynamics (MD) simulations, absorption, distribution, metabolism, excretion, and toxicity (ADMET) analysis, followed by *in vitro* target evaluations using a cell-free C5aR1 inhibition assay. Apoptosis, downstream assessment was carried out by flow cytometry using the HK-2 cells.

Results: The *in silico* screening and ADMET analysis identified C5R-131 as a promising C5aR1 antagonist with favorable pharmacokinetic properties. MD simulations revealed stable binding of C5R-131 to C5aR1, with strong hydrogen bonding interactions, with a binding value of –9.4 kcal/mol. Molecular Mechanics Poisson–Boltzmann Surface Area (MMPBSA)-based binding free energy calculation from the 100 ns simulation trajectories shows C5R-131 has –21.11 kcal/mol when bound to C5aR1. *In vitro* assays demonstrated that C5R-131 significantly inhibited C5aR1 activity with a half-dose inhibitory concentration (IC_{50}) value of 53.75 nM. The compound reduced apoptosis, necrosis, STAT3 phosphorylation, and modulated CD31 expression in high-glucose-exposed HK-2 cells, indicating its potential to protect against renal cell injury and inflammation in DKD.

Conclusion: Through a combination of *in silico* screening and *in vitro* validation, we demonstrate that C5R-131 effectively modulates STAT3 activation, reduces renal cell apoptosis, and protects endothelial cells from dysfunction in high glucose (HG) conditions. These findings offer a new therapeutic strategy for developing targeted therapies for DKD and other diseases associated with C5a receptor activation.

Keywords: Diabetic Kidney Disease; C5a-C5aR1 signaling; C5R-131; STAT3 phosphorylation; virtual screening

Introduction

Diabetic Kidney Disease (DKD) is a significant global health challenge, representing one of the leading causes of chronic kidney disease (CKD) and end-stage renal failure [1,2]. Characterized by progressive renal dysfunction, glomerulosclerosis, and tubulointerstitial fibrosis, DKD is primarily driven by chronic hyperglycemia, inflammation, and impaired kidney function [3,4]. High glucose (HG) levels induce oxidative stress, advanced glycation end product (AGE) accumulation, and activation of protein kinase C (PKC), all of which contribute to inflammation, endothelial dysfunction, and glomerular injury [5]. The pathophysiology of DKD involves complex interactions between various inflammatory and fibrotic pathways. One of the key factors contributing to these processes is the activation of the complement system, specifically complement component 5a (C5a), a pro-inflammatory cytokine generated during complement activation [6,7]. C5a, a potent complement-derived anaphylatoxin, is critically involved in the progression of DKD by driving inflammation, facilitating immune cell infiltration, and promoting tissue injury [8,9]. In particular, C5a exacerbates renal damage in DKD by impairing mitochondrial metabolic flexibility and triggering signal transducer and activator of transcription 3 (STAT3) signaling pathways in glomerular endothelial cells, which may also contribute to dysregulation of the gut-kidney axis [10,11].

A central mediator of inflammation and fibrosis in DKD is the STAT3 pathway, which regulates several cellular processes, including cell survival, proliferation, and the inflammatory response [12]. STAT3 activation in renal cells is triggered by cytokines such as interleukin-6 (IL-6) and growth factors like transforming growth factor beta

(TGF-β), and it has been shown to contribute significantly to kidney fibrosis and glomerulosclerosis [13]. In DKD, STAT3 is activated by C5a, and its activation leads to a pro-inflammatory and pro-fibrotic environment in the kidney [14]. Given the role of C5a and STAT3 in the progression of DKD, targeting the C5a-C5a Receptor 1 (C5aR1) axis and modulating STAT3 signaling represents a promising therapeutic strategy to mitigate kidney damage and prevent disease progression [15].

Current treatment strategies for DKD focus on controlling blood glucose and blood pressure to slow disease progression. Angiotensin-converting enzyme inhibitors (ACE inhibitors) [16], Angiotensin receptor blockers (ARBs) [17], and sodium-glucose cotransporter-2 (SGLT2) inhibitors [18]. They are the most commonly prescribed medications. While these therapies are effective in managing the symptoms and delaying progression, they do not address the underlying inflammation and fibrosis associated with the disease. This gap underscores the need for innovative therapies that go beyond symptom management to target the pathogenic mechanisms of DKD. More targeted approaches are needed to mitigate the inflammatory and fibrotic processes that drive DKD progression. Compounds targeting the C5a-C5aR1 axis have shown promise in preclinical studies, where C5aR1 antagonists have been found to reduce inflammation and fibrosis in various disease models [19]. Importantly, this strategy represents a mechanistically distinct approach from current therapies by directly modulating the immune-mediated injury implicated in DKD. Such interventions may offer disease-modifying potential rather than merely slowing progression. Additionally, targeting STAT3, a key mediator of inflammation and fibrosis, has been explored as a therapeutic strategy. Inhibitors of STAT3 phosphorylation have demonstrated efficacy in reducing fibrosis and improving renal function in experimental models of CKD, including DKD. This approach offers a novel angle by intervening in intracellular signaling pathways central to disease pathology, positioning STAT3 inhibition as a promising candidate for clinical translation [13,20,21].

In this study, we employed an *in silico*-guided approach to identify potential small-molecule inhibitors of C5aR1. High-throughput virtual screening (HTVS) was utilized to screen a diverse chemical library for compounds that could effectively block the C5a-C5aR1 interaction. The screening was followed by computational analysis to assess the binding affinity and stability of the identified compounds, which were further validated through *in vitro* assays. The combination of *in silico* drug discovery techniques and *in vitro* experimental validation allowed for the identification of novel inhibitors with the potential to modulate C5a-C5aR1 and further downstream signaling.

The use of an *in silico*-guided approach also underscores the importance of computational tools in modern drug discovery, allowing for the rapid identification and development of targeted treatments for complex diseases like DKD [22,23]. This study introduces a novel *in silico*-guided approach for the identification of small molecule inhibitors targeting the C5a-C5aR1 signaling axis, a previously underexplored pathway in the treatment of DKD. By combining computational drug discovery with *in vitro* validation, we provide new insights into the potential of C5aR1 inhibitors in modulating STAT3 activation and reducing kidney inflammation, fibrosis, and apoptosis in DKD. This work represents a preliminary basis for further innovative strategies to develop targeted therapies that address both the inflammatory and fibrotic processes in DKD, offering a promising approach to improve patient outcomes in this debilitating disease.

Materials and Methods

Materials

Standard compound PMX53 (#219639-75-5) was purchased from Sigma Aldrich (St. Louis, MO, USA). C5R-131 (# 5858126) was purchased from ChemBridge in San Diego, CA, USA. HK-2 cells (CRL-2190) were provided by The American Type Culture Collection (Rockville, MD, USA). The C5aR1 inhibition kit (# BAH-C5AR11-C5-1) was obtained from RayBiotech Life, Inc. (Peachtree Corners, GA, USA). Phospho-STAT3 (Tyr705) Monoclonal Antibody -PE (# 12-9033-42), CD31 (PECAM-1) Monoclonal Antibody (390), FITC (# 11-0319-42), and the Annexin V kit (# V13242) were from ThermoFisher, Grand Island, NY, USA.

Methods

Structural Analysis of C5a

The Cryo-EM structure of C5aR1 was retrieved from the Protein Data Bank (PDB) database (7Y67). The binding interface between C5a and Guanine nucleotide-binding protein G(i) subunit alpha-1 (GNAI1) was identified using Discovery Studio Visualizer. Receptor cavity prediction analysis was performed using Discovery Studio Visualizer to locate potential druggable pockets within the C5aR1 protein [24].

High-throughput Virtual Screening

A diversity-based HTVS was performed as described previously [25]. Using the ChemBridge compound library, containing approximately 850,000 molecules, as the source of screening compounds, using the Autodock-Vina algorithm from the SiBioLEAD server. The docking grid box was kept at the predicted ligand binding cavity with 20 Å on all sides. The binding affinities of the compounds were evaluated and ranked based on the docking scores.

Absorption, Distribution, Metabolism, Excretion, and Toxicity (ADMET) Predictions

The ADMET properties were assessed using the absorption, distribution, metabolism, excretion, and toxicity-Artificial Intelligence (ADMET-AI) platform (https://admet.ai.greenstonebio.com/) [26]. Initially, compounds were submitted to the platform for analysis after being converted to Simplified Molecular Input Line Entry System (SMILES) format. The pharmacokinetic features, such as tissue distribution, metabolic stability, absorption efficiency, and possible toxicity, were all predicted in detail by the method. To make it easier to compare and choose molecules with the best drug-like properties, these predictions were represented graphically.

Molecular Dynamics Simulation

Molecular dynamics (MD) simulations were carried out as described elsewhere [27]. The investigation was conducted using the GROMACS software suite through the SiBioLEAD MD simulation platform. To simulate the solvent environment, the C5a-C5R-131 complex was submerged in a solvated triclinic box filled with Simple Point Charge (SPC) water molecules. To neutralize the system, sodium chloride (NaCl) was introduced at a physiological concentration of 0.15 M after the system was parameterized using the optimized potentials for liquid simulations (OPLS) force field. The simulation system underwent an initial energy minimization step using the steepest descent algorithm for 5000 steps, aimed at eliminating steric clashes and optimizing the geometry of the system. After energy minimization, a two-phase equilibration process, i.e., NVT (constant volume and temperature), and NPT (constant pressure and temperature), was performed under isothermal-isobaric conditions (300 K, 1 bar) for 300 ps to allow the system to stabilize before running the production simulations. The C5a-C5R-131 complex's conformational stability was evaluated by running production simulations for 100 ns, using the leap-frog integrator, and analyzing the trajectory data for several metrics, including Root Mean Square Deviation (RMSD). Additionally, detailed analyses were conducted on hydrogen bonds and hydrophobic interactions between C5R-131 and C5aR1 to assess the consistency and strength of the binding. These analyses provided insights into the stability of the inhibitor within the C5aR1 binding pocket, supporting the potential of C5R-131 as a promising therapeutic agent for modulating C5a-C5aR1 signaling.

Cell Free C5aR1 Inhibition Assay

In short, test wells pre-coated with C5aR1 were added with 100 µL Log dilutions (0.1 nM to 10,000 nM) of C5R-131 or the standard PMX53 combined with ligand protein concentrate at the required final concentrations. One hundred microliters of diluent solution were added to the blank wells. At room temperature, the plate was incubated for two and a half hours. After this incubation, 100 µL of 1× detection antibody was added to each well, and the wells were then rinsed four times with 1× wash buffer before being left to incubate for an hour at room temperature. After four washes with 1× wash buffer, 1× Horseradish Peroxidase (HRP)-Conjugated anti-Immunoglobulin G (IgG) solution was added to each well, and the wells were incubated for an hour. Following four rounds of washing with 1× wash buffer, each well received 100 µL of 3,3′,5,5′-Tetramethylbenzidine (TMB) One-Step Substrate Reagent, which was then incubated for an additional half hour. A FLUOstar Omega microplate reader (BMG LABTECH, CARY, NC, USA) was used to measure absorbance at 450 nm after 50 µL of stop solution was added directly to each well to stop the color generation. GraphPad Prism software (version 6.0, GraphPad Software, Inc., La Jolla, CA, USA) was used to compute and analyze the % inhibition of kinase activity after subtracting blank data. Values for the half-dose inhibitory concentration (IC_{50}) were displayed.

Cell Viability Assay

Cells used in this study were authenticated by short tandem repeat (STR) profiling and routinely tested for mycoplasma contamination using polymerase chain reaction (PCR)-based assays. Only mycoplasma-free and STR-validated cells were used for all experimental procedures. Before proceeding with the DKD model, we assessed the tolerated dose of C5R-131 in HK-2 cells by analyzing the cell viability. HK-2 cells were cultured in Dulbecco's Modified Eagle Medium/Nutrient Mixture F-12 (DMEM/F12) medium (ThermoFisher, Grand Island, NY, USA) supplemented with 10% fetal bovine serum (FBS), 1% penicillin-streptomycin-amphotericin B, 1% L-glutamine, and 1% insulin-transferrin-selenium (ITS) supplement (ThermoFisher, Grand Island, NY, USA). As reported before, the (3-(4, 5-dimethylthiazolyl-2)-2, 5-diphenyltetrazolium bromide) assay (MTT assay) was employed to determine cell viability. The cells were seeded in 96-well plates (5×10^3 cells/well) and treated with different concentrations of C5R-131 for 72 hours. Following that, the cells were treated with 1 mg/mL MTT (#M2003, Sigma Aldrich, USA), incubated for 4 hours, and then dissolved in dimethyl sulfoxide (DMSO). The absorbance was measured at 560 nm using a FLUOstar Omega microplate reader (BMG LABTECH, CARY, NC, USA). The percentage of viable cells relative to the untreated control was presented.

Apoptosis Assessment

We mimicked DKD using high glucose (HG) conditions as described elsewhere [28] to evaluate the necrosis/ apoptosis post-C5aR1 inhibition by C5R-131. The cell culture medium was switched to DMEM normal glucose (NG, 5.5 mM glucose, ThermoFisher, Grand Island, NY, USA) one week before the start of the experiments.

A 10% FBS supplement was added, along with 1% penicillin/streptomycin/amphotericin B, 1% glutamine, and 1% insulin-transferrin-selenium (ITS) (ThermoFisher, Grand Island, NY, USA). HK-2 cells at a concentration of 2.5 $\times$ 10^5 were seeded and cultivated to 90% confluence for the experiments. After C5R-131 treatments, cells were exposed to medium DMEM NG or DMEM high glucose (HG, 25 mM glucose, ThermoFisher, Grand Island, NY, USA) for 24 hours, supplemented with 0.5% FBS, 1% penicillin/streptomycin/amphotericin B, 1% glutamine, and 1% ITS. After the incubation period, the cells were stained with 0.25 µg/mL Annexin V reagent, 0.5 µg/mL propidium iodide (PI) for 15 minutes in the dark after a couple of washes using the kit's buffer and resuspended in Hank's Balanced Salt Solution (HBSS) buffer. To differentiate between healthy, apoptotic, and necrotic cells, flow cytometry was performed by collecting data from 1 $\times$ 10^3 events using a Guava easyCyte system (Guava easyCyte™ HT System, Merk Millipore, Billerica, MA, USA). The results were then examined using InCyte software (version 2.7, Merk Millipore, MA, USA). GraphPad Prism software (version 6.0, GraphPad Software, Inc., La Jolla, CA, USA) was used to present the results.

STAT3 Inhibition and CD31 Expression Assay (Flow Cytometry)

As mentioned in the previous section, HK-2 cells were grown in both NG and HG environments. Cells were taken off the plates and placed in sterile Eppendorf tubes after being treated for 24 hours with different concentrations of C5R-131. After 10 minutes of 4% formaldehyde fixation, the cells were subjected to a 15-minute treatment with 90% methanol at –20 °C. After that, the cells were cultured in 10% normal goat serum and 1$\times$ HBSS buffer to prevent non-specific protein-protein interactions. The cells were stained with Phospho-STAT3 (Tyr705) Monoclonal Antibody -PE (0.06 µg) or CD31 (PECAM-1) Monoclonal Antibody (390), FITC (0.5 µg) for 15 minutes in the dark. Back in the HBSS buffer. The cells were suspended once again in the HBSS solution following two washes to remove any residual dye. Five thousand events were collected using a Guava easyCyte flow cytometer system (Guava easyCyte™ HT System, Merk Millipore, MA, USA). Using Millipore's InCyte software (version 2.7, Merk Millipore, MA, USA), analysis was performed to determine the proportion of positive populations to compare to the untreated controls.

Statistical Analysis

All data were analyzed using GraphPad Prism software (version 6.0). Results were expressed as the mean $\pm$ standard deviation (SD) of at least three independent experiments. Statistical comparisons between groups were performed using one-way/two-way analysis of variance (ANOVA) followed by Tukey's multiple comparison test, with $*p < 0.05$ considered statistically significant.

Results

Structural Analysis of C5aR1 Protein Complex

To identify novel small molecule inhibitors against C5aR1 activity, we first examined the structural interaction between C5aR1 and other proteins, i.e., GNAI1. The Cryo-EM structure of C5aR1 was analyzed (Fig. 1a). The results show the complex between C5aR1 (white) and the Guanine nucleotide-binding protein G(i) subunit alpha-1 (GNAI1; green), illustrating the binding interface between the two proteins. Fig. 1b presents the interaction analysis of C5a, highlighting the region (yellow) that is critical for interactions with GNAI1. This analysis identifies specific residues of C5aR1 that play a pivotal role in the formation of the complex. Based on this, we analyzed the presence of a druggable pocket within the C5aR1 protein through receptor cavity prediction analysis. Results show a large pocket (Fig. 1c; green mesh) in C5aR1. This pocket is suggested as a potential target for therapeutic intervention.

High-throughput Virtual Screening

To identify novel lead molecules for C5aR1 and to evaluate the docking potential, a diversity-based HTVS analysis was conducted for the ChemBridge library against C5aR1. Results show the predicted docking energies (Fig. 2). The histogram in Fig. 2a illustrates the distribution of docking energies, highlighting a broad range of binding affinities among the compounds. Several compounds demonstrate low predicted docking energies, suggesting stronger interactions with C5aR1, while others exhibit higher energies, indicating weaker binding. Fig. 2b displays the predicted docking energies for the top 5 compounds, which were identified as having the most favorable interactions with C5aR1, based on their lower docking energy values. These compounds show potential as high-affinity binders, making them strong candidates for further investigation.

ADMET Predictions Identify C5R-131 as a Lead Molecule

To identify the best lead compound for C5aR1, we performed ADMET calculations for the top 5 predicted compounds against C5aR1. Results show the ADMET properties (Fig. 3), including absorption, distribution, metabolism, excretion, and toxicity predictions, derived from ADMET-AI analysis. Fig. 3a–e provide a detailed overview of the predicted ADMET profiles for each compound. The analysis reveals that compound C5R-131 exhibited a favorable pharmacokinetic property, such as high absorption rates, favorable distribution characteristics, and low toxicity potential. Comparing the docking scores and the ADMET-AI predictions C5R-131 is a better lead molecule than C5R-130 or C5R-091 to pursue forward, therefore selected for further evaluations.

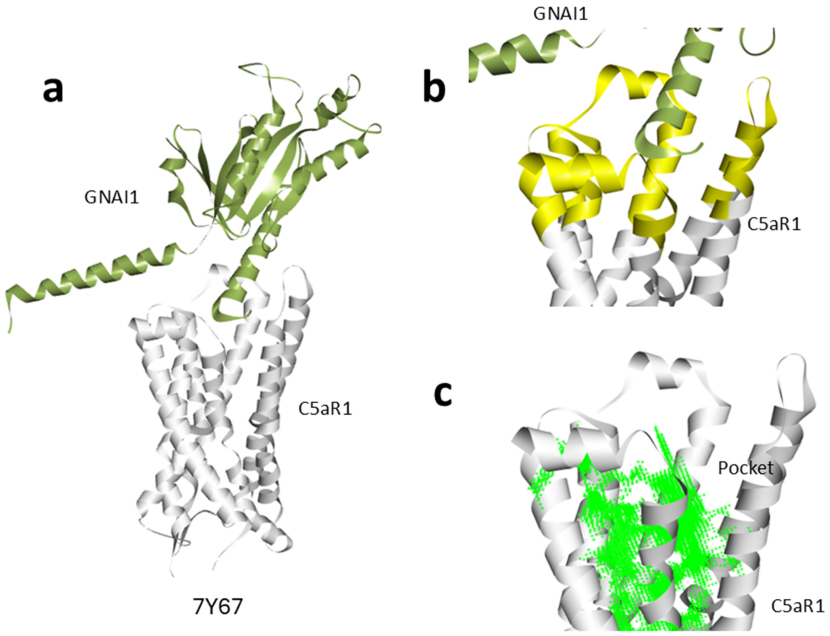

Fig. 1. Structure of C5aR1. (a) Retrieved Cryo-EM structure of C5aR1 showing the complex between C5aR1 (white) and Guanine nucleotide-binding protein G(i) subunit alpha-1 (GNAI1; green). (b) C5aR1 interaction analysis highlighting the region of importance in C5aR1 participating in interactions with GNAI1 protein (highlighted in yellow). (c) Presence of a druggable pocket in the C5aR1 protein identified through Receptor cavity prediction analysis. C5aR1, complement component 5a Receptor 1.

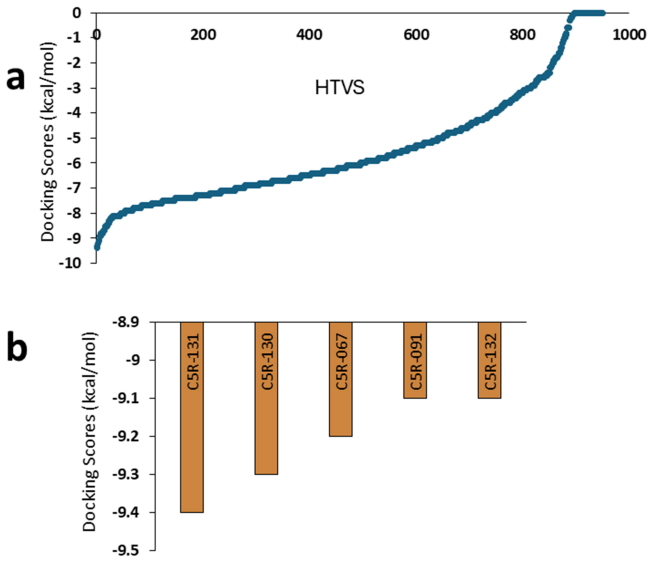

Fig. 2. High-throughput virtual screening. (a) Histogram representing the predicted docking energies for ChemBridge compounds against complement component 5a (C5a) based on Diversity-based high-throughput virtual screening (HTVS) analysis. (b) Predicted docking energies for the top 5 compounds.

Protein-ligand Interaction Analysis of C5R-131::C5aR1 Complex

To investigate the protein-ligand interactions of C5R-131 with C5aR1, docking studies were performed to predict the binding pose of C5R-131. Results show the predicted docking pose for C5R-131 bound to C5aR1 at its predicted ligand binding cavity (Fig. 4a). The docking analysis reveals the positioning of C5R-131 within the cavity, suggesting key interactions. Fig. 4b presents the protein-ligand interaction analysis of C5R-131 in complex with C5aR1, highlighting the amino acid interactions that stabilize the complex. This analysis identifies crucial residues of C5aR1 involved in ligand binding. Additionally, Fig. 4c provides a 2D representation of the interactions between C5R-131

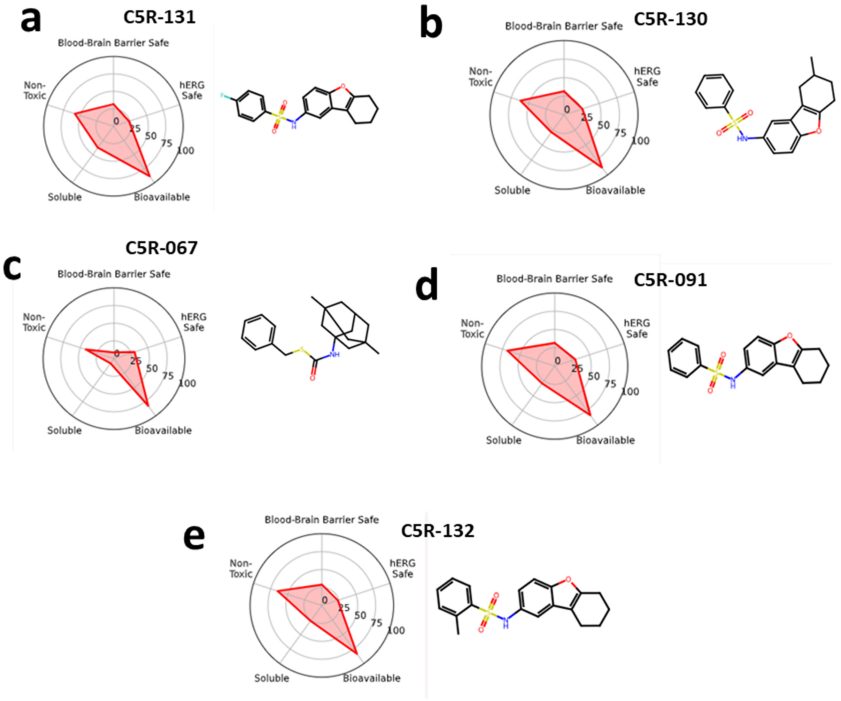

Fig. 3. ADMET property prediction. (a–e) ADMET-AI-based predictions for the top 5 predicted compounds against C5aR1. ADMET-AI, absorption, distribution, metabolism, excretion, and toxicity-Artificial Intelligence.

and the amino acid residues of C5aR1, illustrating the specific contacts and interactions at the interface of the complex. The 2D interaction map highlights key amino acids, including VAL 247, ILE 299, TYR 222, and others, interacting with the ligand (Fig. 4c).

Molecular Dynamics Simulation of C5R-131::C5aR1 Complex

To assess the stability of the C5R-131 binding to C5aR1, a molecular dynamics (MD) simulation was conducted over a 100-ns timespan. Fig. 5a,b show snapshots of simulation trajectory frames taken before and after the 100 ns simulation, respectively, illustrating that C5R-131 binds stably at the predicted pocket in the C5aR1 protein. The binding stability of C5R-131 within the binding cavity is maintained throughout the simulation, suggesting a stable interaction between the ligand and protein. Fig. 5c presents the predicted ligand Root Mean Square Deviation (RMSD) for C5R-131, calculated from the 100 ns simulation trajectories. The RMSD data reveal that C5R-131 exhibits minimal deviation, indicating a stable binding pose within the C5aR1 binding pocket throughout the simulation period. Fig. 5d illustrates the predicted protein-ligand hydrogen bonds (h-bonds) for the 100 ns simulation, calculated from the simulation trajectories. The analysis highlights the formation of stable hydrogen bonds between C5R-131 and key amino acids of the C5aR1 protein, contributing to the overall stability of the complex. Molecular Mechanics Poisson–Boltzmann Surface Area (MMPBSA)-based binding energy calculation from the 100 ns simulation trajectories shows C5R-131 has –21.11 kcal/mol when bound to C5aR1 (Fig. 5e).

Dose-dependent Inhibition of C5aR1 by C5R-131

The inhibitory activity of C5R-131 was assessed using a cell-free enzyme assay kit to validate the computational predictions. With an IC_{50} value of 53.75 ± 17.91 nM, C5R-131 efficiently suppressed the C5aR1 activity (Fig. 6a). The IC_{50} value of PMX53, a common C5aR1 inhibitor, was 18 ± 4.41 nM (Fig. 6b). We used the near IC_{25}, IC_{50}, and IC_{100} doses C5R-131 (25 nM, 50 nM, and 100 nM, respectively) for dose-dependent studies in the following cellular experiments. We also checked the effect of PMX53 on the viability of HK-2 cells. The viability of HK-2 cells was unaltered from 0 to 3000 nM (Fig. 6c). However, a significant reduction (* $p < 0.05$) in the viability of the HK-2 cells at 5000 nM and 10,000 nM treatments of PMX53 was observed (Fig. 6c). The non-toxic dose level of 3000 nM was very much higher than the PMX53 concentrations (25 nM, 50 nM and 100 nM) which was tested in other assays.

C5R-131 Treatment Protects Against Apoptosis in HG-exposed HK-2 Cells

Prior, the effect of the compound on normal HK-2 cells was assessed using the MTT assay for determining the cell viability. C5R-131 did not alter the viability of these cells up to 3000 nM and lower concentrations tested (Fig. 6c). Apoptosis was assessed to determine the protec-

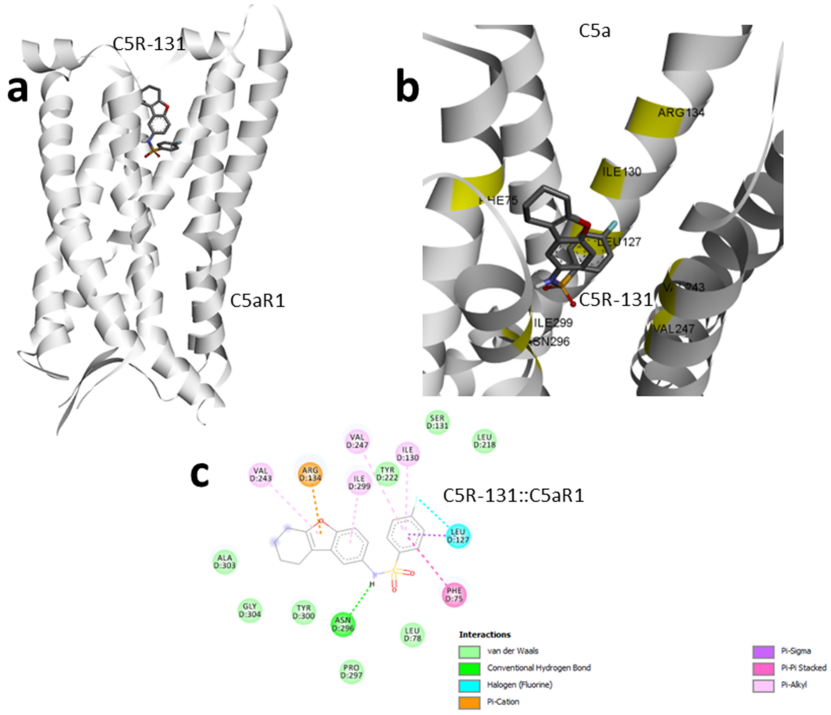

Fig. 4. Protein-ligand interaction analysis of C5R-131. (a) predicted docking pose for C5R-131 bound to C5aR1 at its predicted ligand binding cavity. (b) Protein-ligand interaction analysis of C5R-131 in complex with C5aR1 protein showing amino acid interactions. (c) 2D representation of C5R-131 interactions with amino acid residues of C5aR1.

tive effects of C5R-131 in the HG-induced HK-2 cells using flow cytometry (Fig. 7a). The results demonstrated that HG exposed HK-2 cells showed 27.9% early and 11.6% late apoptosis cells after 24 hours (Fig. 7b). The number of necrotic populations was 5.65% in HG-exposed HF-2 cells after 24 hours. These numbers were significantly higher (*** $p < 0.001$) than the normal glucose (NG) exposed HF-2 cells at 24 h, which had 2.89%, 2.1%, and 1.1% early apoptosis, late apoptosis, and necrotic cells, respectively (Fig. 7b). Treatment with near IC_{25}, IC_{50}, and IC_{100} doses of C5R-131 dose dependently reduced the proportion of early apoptotic, late apoptotic, and necrotic cells compared to the untreated HG exposed control HK-2 cells (Fig. 7a). Treatment with 25 nM C5R-131 reduced early apoptosis and late apoptosis to 14.84% and 8.04% respectively, in these cells (Fig. 7b). The necrotic population in 25 nM C5R-131-treated HG-HK-2 cells was 2.21% (Fig. 7b). A similar pattern of further significant reduction in the early phase apoptosis, late phase apoptosis, and necrosis was observed at 50 nM and 100 nM treatments of C5R-131 (Fig. 7a,b) (** $p < 0.01$).

C5R-131 Inhibited STAT3 Activation and Reduced the DKD Marker CD31 in HG-HK-2 Cells

To assess the effect of C5R-131 on STAT activation, a flow cytometry-based STAT3 assay was conducted. HK-2 cells exposed to HG medium were treated with C5R-131 and compared with NG HK-2 cells (Fig. 8a). The percentage of positive phospho-STAT3 HK-2 cells was then analyzed. After 24 h, the normal glucose (NG) HK-2 cells had a 1.38% positive population of p-STAT3 cells, while HG-HK-2 cells had a significant increase (*** $p < 0.001$) of 23.84% p-STAT3 positive cells (Fig. 8b). Treatment with 25 nM, 50 nM, and 100 nM of C5R-131 significantly reduced (** $p < 0.01$) the percentage of positive p-STAT3 cells to 10.13%, 7.16%, and 2.53%, respectively (Fig. 8b). On the other hand, the normal glucose (NG) HK-2 cells had 65.66% positive population of CD31 cells, while HG-HK-2 cells had a significant reduction (* $p < 0.05$) of 23.78% CD31 positive cells (Fig. 9a,b). Treatment with 25 nM, 50 nM, and 100 nM of CD31 significantly (* $p < 0.05$) increased the percentage of positive CD31 cells to 41.04%, 48.90%, and 60.16%, respectively (Fig. 9a,b).

Discussion

C5a, through its receptor C5aR1, plays a critical role in the pathogenesis of DKD. In DKD, C5a contributes to both glomerular injury and tubulointerstitial fibrosis, two hallmark features of kidney dysfunction [29]. The C5a-C5aR1 axis regulates immune cell recruitment, endothelial dysfunction, and the activation of signaling pathways that exacerbate kidney damage [30]. C5a promotes the infiltration of neutrophils, macrophages, and other immune cells into the kidney, amplifying the inflammatory response. Moreover, C5a directly activates fibroblasts and renal tubu-

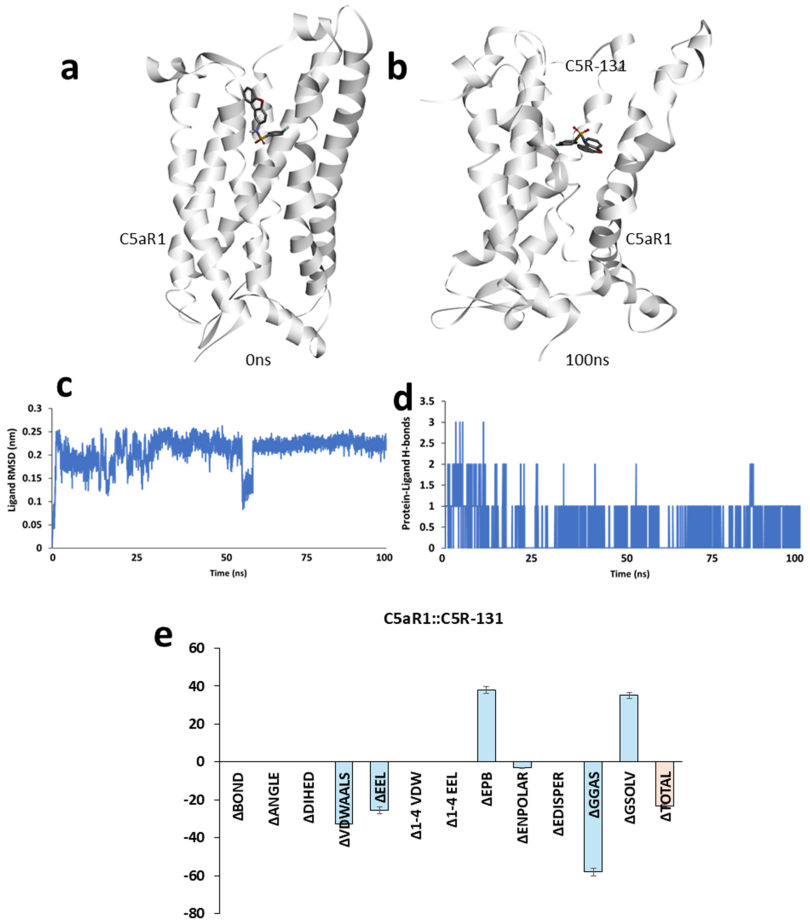

Fig. 5. Molecular Dynamics simulation. (a) Snapshots of simulation trajectory frames taken before (a) and after (b) 100 ns simulation show C5R-131 binds stably at the predicted pocket in C5aR1 protein. (c) Predicted ligand Root Mean Square Deviation (RMSD) for C5R-131 calculated from 100 ns simulation trajectories. (d) Predicted protein-ligand h-bonds for 100 ns simulation calculated from simulation trajectories. (e) Molecular Mechanics Poisson–Boltzmann Surface Area (MMPBSA)-based binding energy calculation of 100 ns simulation trajectories predicts Gibbs binding free energy estimates for C5R-131 in complex with C5aR1. Δ, energy change.

lar cells, leading to increased production of extracellular matrix components and fibrosis [31]. This scarring of kidney tissue results in progressive loss of renal function and the development of DKD. Targeting C5a with C5R-131 offers a promising strategy to slow or prevent DKD progression by reducing inflammation, immune activation, and fibrosis.

Structural analysis of C5a revealed its complex formation with the Guanine nucleotide-binding protein G(i) subunit alpha-1 (GNAI1), which plays a role in signaling pathways related to inflammation and cell survival. The structural data highlighted a druggable pocket within C5aR1, making it a viable target for therapeutic intervention. This discovery supports the development of small molecules, such as C5R-131, which can block the C5a-C5aR1 interaction, thereby interrupting the signaling pathway critical for the progression of DKD [11]. The identification of this pocket within C5aR1 offers valuable insight into the design of targeted inhibitors that may have therapeutic potential in kidney diseases.

Through HTVS, this study identified several lead compounds, with C5R-131 emerging as a top candidate. ADMET analysis confirmed C5R-131 to possess favorable pharmacokinetic properties, such as high absorption rates, favorable distribution characteristics, and low toxicity. Based on its favorable ADMET properties, C5R-131 shares similarities with SGLT2 inhibitors like empagliflozin and canagliflozin, which are used to treat DKD by reducing inflammation and fibrosis [32]. Like SGLT2 inhibitors, C5R-131 targets inflammatory pathways, offering a complementary approach to current therapies. Its promising ADMET profile suggests it could provide therapeutic benefits with minimal adverse effects in DKD treatment. These properties make C5R-131 a therapeutic candidate for further development targeting C5a in DKD [33]. The ADMET profile supports the potential of C5R-131 for oral bioavailability and therapeutic use, offering a favorable alternative to more invasive treatment options [34].

The protein-ligand interaction analysis and molecular dynamics (MD) simulations further confirmed the stable

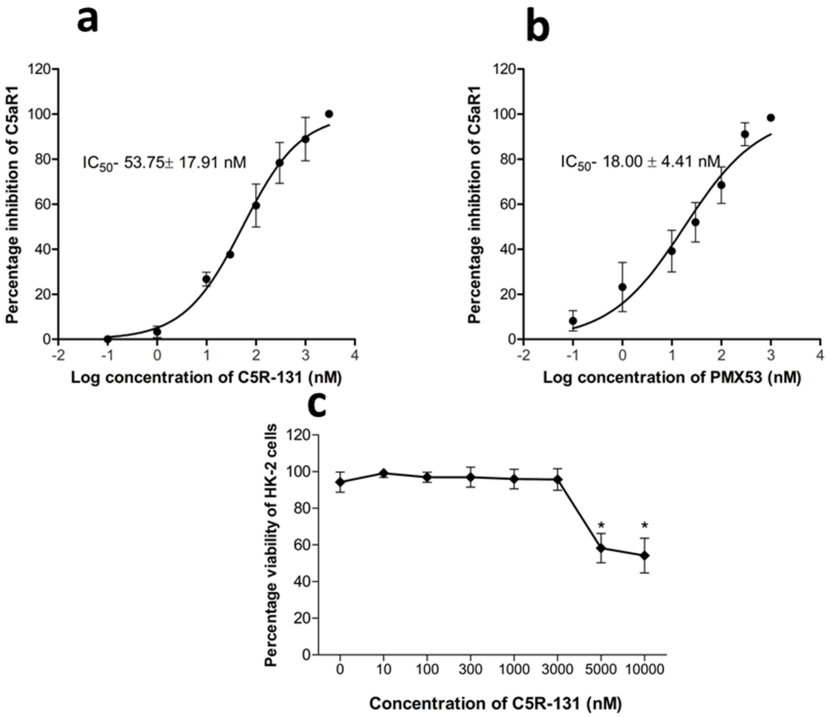

Fig. 6. Efficacy of C5R-131 against C5aR1 kinase activity. (a) Variable concentrations (0.1 nM to 10,000 nM) of C5R-131 or (b) the standard compound PMX53 were tested against the activity of C5aR1, and the IC_{50} values were determined. Results expressed as mean ± SD from three experiments were analyzed using GraphPad Prism version 6.0 software. (c) The effect of C5R-131 doses on the viability of HK-2 cells was presented. The MTT assay was used to assess viability, using GraphPad Prism version 6.0 software. The results are expressed as mean ± SD from three experiments in duplicates. Statistically significant at * $p < 0.05$.

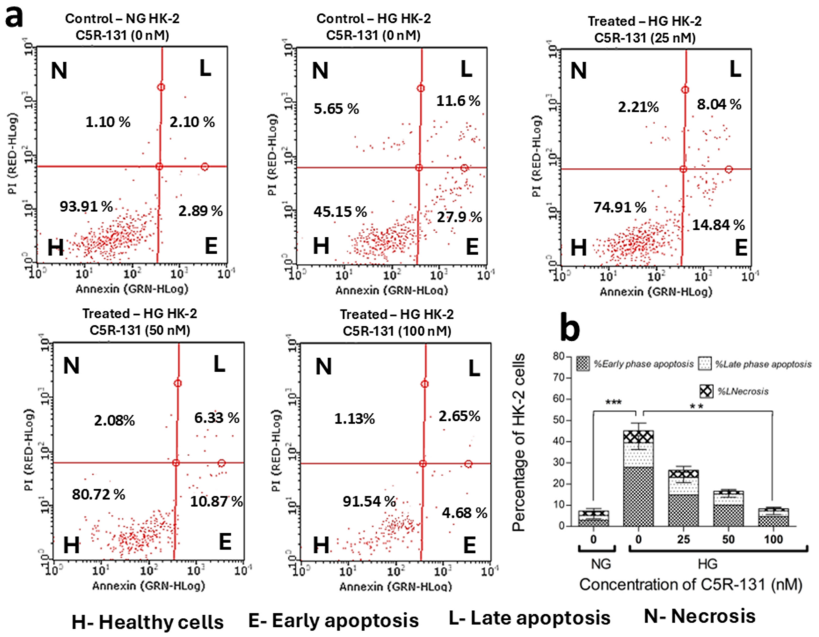

Fig. 7. Effect of C5R-131 on high-glucose (HG)-exposed HK-2 cells. (a) At 24 h, HG exposure promoted early-phase, late-phase apoptosis and necrosis in HK-2 cells when compared to the NG HF-2 cells. Treatment of C5R-131 dose dependently decreased the apoptotic and necrotic population in HG-exposed HK-2 cells. All tests were conducted three times, and representative plots were provided. (b) Enumeration of early phase, late phase apoptosis and necrosis levels in NG exposed and HG exposed untreated, C5R-131 treated HF-2 cells. The results are expressed as mean ± SD and are statistically significant at *** $p < 0.001$, ** $p < 0.01$.

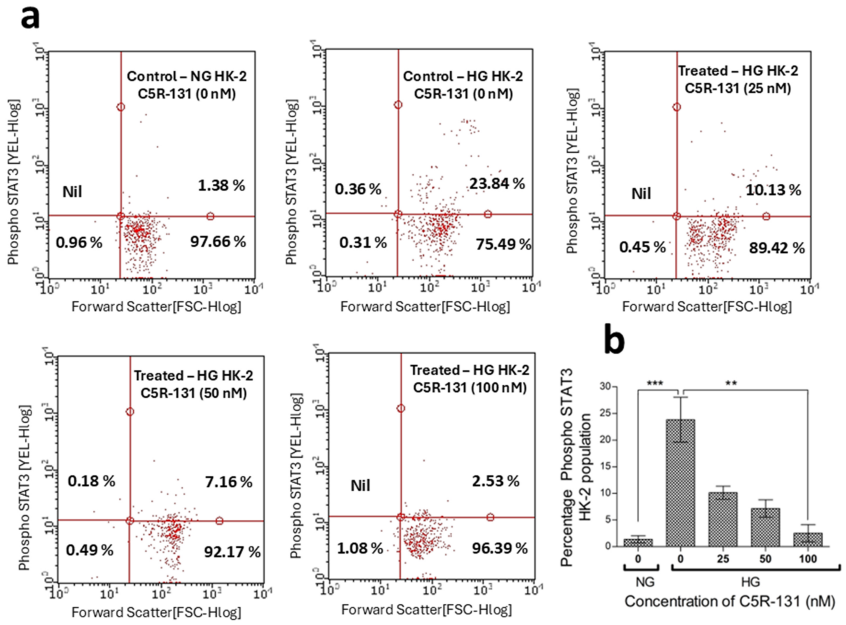

Fig. 8. Phospho-signal transducer and activator of transcription 3 (STAT-3) positive population in HG exposed HF-2 cells was suppressed by C5R-131. (a) The endogenous Phospho-STAT-3 population was increased upon exposure to HG in HF-2 cells, which was reduced by C5R-131 treatments when compared to the respective untreated HG-exposed control cells. Representative graphs are presented. (b) Numerical values are mean ± SD from three individual experiments. Statistical significance at *** $p < 0.001$, ** $p = 0.01$.

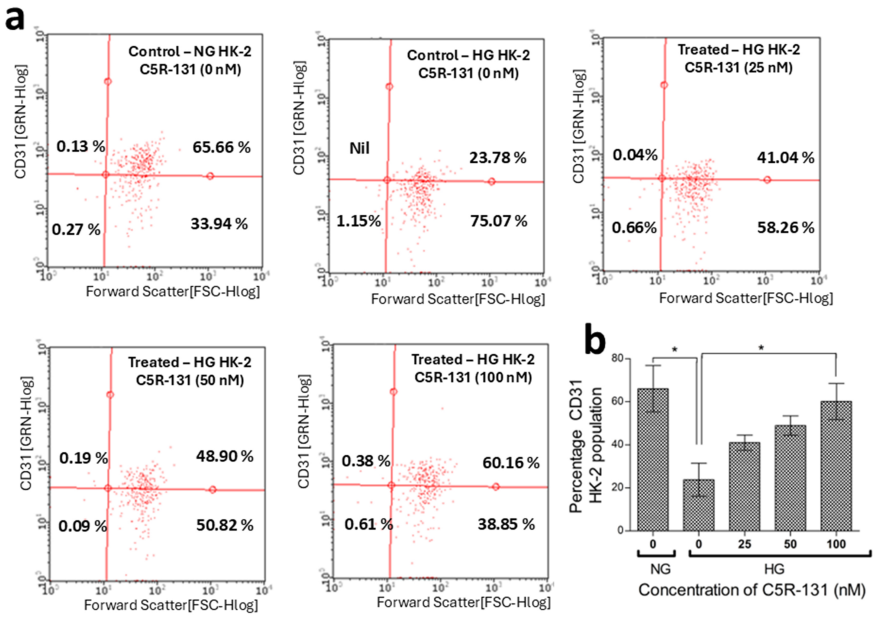

Fig. 9. CD-31 positive population in HG exposed HF-2 cells was suppressed by C5R-131. (a) The endogenous CD-31 population was increased upon exposure to HG in HF-2 cells, which was reduced by C5R-131 treatments when compared to the respective untreated HG-exposed control cells. Representative graphs are presented. (b) Numerical values from the graph are expressed as mean ± SD from three individual experiments. Statistical significance at * $p < 0.05$.

binding of C5R-131 to C5aR1. The stability of the C5R-131-C5aR1 complex was maintained throughout the 100ns simulation, indicating that C5R-131 binds strongly to C5a and remains stable over time [35]. The formation of hydrogen bonds between C5R-131 and critical residues of C5aR1 contributed to the overall stability of the complex. These findings provide a solid foundation for the continued exploration of C5R-131 as a potential therapeutic inhibitor of

C5a signaling in DKD and other related diseases [8]. Our *in vitro* observations were in par with these computational data, where a dose-dependent C5aR1 inhibition by C5R-131 was observed.

Previous studies have shown that complement activation, especially via the C5a-C5aR1 axis, is a key contributor to DKD progression. C5a enhances leukocyte infiltration, promotes pro-inflammatory cytokine release (such as IL-6, TNF-α), and stimulates profibrotic mediators like TGF-β1, leading to glomerular and tubular damage [36]. Inhibiting C5aR1 would therefore help to overcome cellular damage in DKD. In this context, we mimicked high glucose conditions in HK-2 cells and observed the effect of C5R-131 with relevant to cell integrity, apoptosis, and necrosis. C5R-131 treatment significantly protected HK-2 cells from apoptosis and cell death induced by high glucose. Flow cytometry analysis using Annexin V/PI staining demonstrated that C5R-131 significantly reduced the proportion of apoptotic and necrotic cells compared to untreated HG-exposed control cells. This protective effect suggests that C5R-131 helps preserve kidney cell integrity and function, which is essential for alleviating the progression of DKD. By reducing apoptosis and necrosis [37]. C5R-131 may provide a crucial protective effect against kidney damage induced by chronic hyperglycemia [36].

The STAT3 pathway has been recognized as a critical mediator of inflammation, fibrosis, and cell survival in the DKD. The activation of STAT3, therefore, may contribute to a pro-inflammatory and pro-fibrotic environment, which leads to the progressive kidney damage characteristic of the disease [6]. This pathway is activated by various cytokines such as IL-6 and growth factors like TGF-β, which play a role in regulating cell proliferation, survival, and fibrosis [38]. Studies have demonstrated that C5a, a pro-inflammatory cytokine produced during complement activation, significantly increases STAT3 pathway activation [39,40]. This finding suggests that C5a plays a pivotal role in the inflammatory and fibrotic processes observed in DKD. Our results indicate that C5R-131 effectively inhibit STAT3 phosphorylation. While C5R-131 inhibits STAT3 phosphorylation, its impact on renal fibrosis and inflammation may be attributed to STAT3's role in regulating pro-inflammatory cytokine production, cell survival, and the activation of fibrotic pathways. By preventing STAT3 activation, C5R-131 likely reduces the expression of key fibrotic markers like TGF-β and collagen, while also modulating the inflammatory response by inhibiting immune cell infiltration and cytokine secretion. By blocking C5a signaling through the C5aR1 [41], C5R-131 may offer therapeutic benefits in treating DKD by disrupting these pathological cascades. In addition to inhibiting C5a-C5aR1 binding, C5R-131 was shown to reduce STAT3 activation in HK-2 cells treated with high glucose, mimicking the diabetic condition [8,11]. The flow cytometry analysis revealed that C5R-131 effectively inhibited STAT3 phosphorylation in a dose-dependent manner, providing compelling evidence for its ability to modulate STAT3 signaling in DKD. This suggests that C5R-131 can mitigate the inflammatory and fibrotic responses in kidney cells, which are key features in the progression of DKD.

Finally, C5R-131 was shown to stabilize CD31 expression, an endothelial cell marker, in HK-2 cells. CD31 functions as a key regulator of leukocyte transmigration, vascular permeability, and endothelial cell integrity. In the context of DKD [42], its expression is dysregulated, playing a contributory role in disease onset and progression [43]. C5a facilitates the endothelial-to-myofibroblast transition (EndMT), a pathological process in which endothelial cells acquire myofibroblast-like characteristics, contributing to renal fibrosis and a corresponding decline in CD31 expression within the glomeruli [44]. Observed increase in CD31 levels suggests that C5R-131 may inhibit endothelial cell activation and modulate the endothelial barrier function [45,46]. Given the significant role of endothelial dysfunction in the pathogenesis of DKD, this finding underscores the therapeutic potential of C5R-131 in mitigating vascular complications. Chronic hyperglycemia in DKD induces endothelial activation, characterized by increased expression of adhesion molecules (e.g., ICAM-1, VCAM-1), enhanced leukocyte adhesion, and disrupted nitric oxide (NO) signaling, all of which contribute to microvascular inflammation and capillary rarefaction. C5a, through its interaction with C5aR1 on endothelial cells, further exacerbates this dysfunction by promoting oxidative stress and pro-inflammatory signaling. By antagonizing C5aR1, C5R-131 may restore endothelial homeostasis, reduce leukocyte-endothelial interactions, and preserve microvascular integrity, thereby playing a critical role in preventing progressive vascular injury and albuminuria associated with DKD.

The findings of this preliminary investigation are limited to the identification of a novel C5aR1 inhibitor, which may be developed as a novel therapeutic drug against DKD. The promising preclinical findings of C5R-131 suggest its potential for translating into clinical practice as a targeted therapy for DKD by modulating key inflammatory and fibrotic pathways. However, challenges in drug development may arise, including the need for thorough clinical testing to confirm its long-term safety, potential off-target effects, and efficacy in diverse patient populations, particularly given the complexity of complement system signaling and the risk of immunosuppression.

Conclusion

In conclusion, C5R-131 was identified as a promising therapeutic candidate for Diabetic Kidney Disease by effectively inhibiting C5a-C5aR1 signaling, reducing STAT3 activation, protecting against apoptosis, and modulating endothelial cell activity. Its favorable pharmacokinetic prop-

erties, strong binding affinity, and protective effects in DKD make it an attractive candidate for further preclinical and clinical development. Further studies are warranted to explore its full therapeutic potential in DKD and other diseases associated with C5a activation.

Availability of Data and Materials

All data were used in this study and any supporting information is available from the corresponding author upon reasonable request.

Author Contributions

AAD and MAS: Conceptualization, methodology, validation, formal analysis, drafting, critically revising, and funding acquisition. Both authors read and approved the final version of the manuscript. Both authors have participated sufficiently in the work and agreed to be accountable for all aspects of the work.

Ethics Approval and Consent to Participate

Not applicable.

Acknowledgment

Not applicable.

Funding

The authors extend their appreciation to the Deanship of Scientific Research at King Khalid University for funding this work through a large group Research Project under grant number (RGP2/154/46).

Conflict of Interest

The authors declare no conflict of interest.

References

[1] Fu H, Liu S, Bastacky SI, Wang X, Tian XJ, Zhou D. Diabetic kidney diseases revisited: A new perspective for a new era. Molecular Metabolism. 2019; 30: 250–263. https://doi.org/10.1016/j.molmet.2019.10.005.

[2] Alicic RZ, Rooney MT, Tuttle KR. Diabetic Kidney Disease: Challenges, Progress, and Possibilities. Clinical Journal of the American Society of Nephrology: CJASN. 2017; 12: 2032–2045. https://doi.org/10.2215/CJN.11491116.

[3] Sinha SK, Nicholas SB. Pathomechanisms of Diabetic Kidney Disease. Journal of Clinical Medicine. 2023; 12: 7349. https://doi.org/10.3390/jcm12237349.

[4] Xu C, Ha X, Yang S, Tian X, Jiang H. Advances in understanding and treating diabetic kidney disease: focus on tubulointerstitial inflammation mechanisms. Frontiers in Endocrinology. 2023; 14: 1232790. https://doi.org/10.3389/fendo.2023.1232790.

[5] González P, Lozano P, Ros G, Solano F. Hyperglycemia and Oxidative Stress: An Integral, Updated and Critical Overview of Their Metabolic Interconnections. International Journal of Molecular Sciences. 2023; 24: 9352. https://doi.org/10.3390/ijms24119352.

[6] Mo GP, Zhu Y, You Y, Chen H, Zhang J, Ku B, *et al*. Diabetic Kidney Disease: Disease Progression Driven by Positive Feedback Loops and Therapeutic Strategies Targeting Pathogenic Pathways. Diabetes, Metabolic Syndrome and Obesity: Targets and Therapy. 2025; 18: 1073–1085. https://doi.org/10.2147/DMSO.S513080.

[7] Rogacka D, Rachubik P, Typiak M, Kulesza T, Audzeyenka I, Saleem MA, *et al*. Involvement of ADAM17-Klotho Crosstalk in High Glucose-Induced Alterations of Podocyte Function. International Journal of Molecular Sciences. 2025; 26: 731. https://doi.org/10.3390/ijms26020731.

[8] Trambas IA, Coughlan MT, Tan SM. Therapeutic Potential of Targeting Complement C5a Receptors in Diabetic Kidney Disease. International Journal of Molecular Sciences. 2023; 24: 8758. https://doi.org/10.3390/ijms24108758.

[9] Ma J, Yiu WH, Tang SCW. Complement anaphylatoxins: Potential therapeutic target for diabetic kidney disease. Diabetic Medicine: a Journal of the British Diabetic Association. 2025; 42: e15427. https://doi.org/10.1111/dme.15427.

[10] Tan SM, Ziemann M, Thallas-Bonke V, Snelson M, Kumar V, Laskowski A, *et al*. Complement C5a Induces Renal Injury in Diabetic Kidney Disease by Disrupting Mitochondrial Metabolic Agility. Diabetes. 2020; 69: 83–98. https://doi.org/10.2337/db19-0043.

[11] Li L, Wei T, Liu S, Wang C, Zhao M, Feng Y, *et al*. Complement C5 activation promotes type 2 diabetic kidney disease via activating STAT3 pathway and disrupting the gut-kidney axis. Journal of Cellular and Molecular Medicine. 2021; 25: 960–974. https://doi.org/10.1111/jcmm.16157.

[12] Liu Y, Wang W, Zhang J, Gao S, Xu T, Yin Y. JAK/STAT signaling in diabetic kidney disease. Frontiers in Cell and Developmental Biology. 2023; 11: 1233259. https://doi.org/10.3389/fcell.2023.1233259.

[13] Pace J, Paladugu P, Das B, He JC, Mallipattu SK. Targeting STAT3 signaling in kidney disease. American Journal of Physiology. Renal Physiology. 2019; 316: F1151–F1161. https://doi.org/10.1152/ajprenal.00034.2019.

[14] Huang R, Fu P, Ma L. Kidney fibrosis: from mechanisms to therapeutic medicines. Signal Transduction and Targeted Therapy. 2023; 8: 129. https://doi.org/10.1038/s41392-023-01379-7.

[15] Xu Z, Tao L, Su H. The Complement System in Metabolic-Associated Kidney Diseases. Frontiers in Immunology. 2022; 13: 902063. https://doi.org/10.3389/fimmu.2022.902063.

[16] Mallik R, Chowdhury TA. Pharmacotherapy to delay the progression of diabetic kidney disease in people with type 2 diabetes: past, present and future. Therapeutic Advances in Endocrinology and Metabolism. 2022; 13: 20420188221081601. https://doi.org/10.1177/20420188221081601.

[17] Tong LL, Adler SG. Diabetic kidney disease treatment: new perspectives. Kidney Research and Clinical Practice. 2022; 41: S63–S73. https://doi.org/10.23876/j.krcp.21.288.

[18] Han S, Kim S. A New Era in Diabetic Kidney Disease Treatment: The Four Pillars and Strategies to Build Beyond. Electrolyte & Blood Pressure: E & BP. 2024; 22: 21–28. https://doi.org/10.5049/EBP.2024.22.2.21.

[19] Fonseca MI, Ager RR, Chu SH, Yazan O, Sanderson SD, LaFerla FM, *et al*. Treatment with a C5aR antagonist decreases pathology and enhances behavioral performance in murine models of Alzheimer's disease. Journal of Immunology (Baltimore, Md.: 1950). 2009; 183: 1375–1383. https://doi.org/10.4049/jimmunol.0901005.

[20] Brosius FC, 3rd, He JC. JAK inhibition and progressive kidney disease. Current Opinion in Nephrology and Hy-

pertension. 2015; 24: 88–95. https://doi.org/10.1097/MNH.0000000000000079.

[21] Liu C, Yang M, Li L, Luo S, Yang J, Li C, *et al*. A Glimpse of Inflammation and Anti-Inflammation Therapy in Diabetic Kidney Disease. Frontiers in Physiology. 2022; 13: 909569. https://doi.org/10.3389/fphys.2022.909569.

[22] Senent Y, Remírez A, Repáraz D, Llopiz D, Celias DP, Sainz C, *et al*. The C5a/C5aR1 Axis Promotes Migration of Tolerogenic Dendritic Cells to Lymph Nodes, Impairing the Anticancer Immune Response. Cancer Immunology Research. 2025; 13: 384–399. https://doi.org/10.1158/2326-6066.CIR-24-0250.

[23] Agamah FE, Mazandu GK, Hassan R, Bope CD, Thomford NE, Ghansah A, *et al*. Computational/in silico methods in drug target and lead prediction. Briefings in Bioinformatics. 2020; 21: 1663–1675. https://doi.org/10.1093/bib/bbz103.

[24] Al Shahrani M, Rajagopalan P, Abohassan M, Alshahrani M, Alraey Y. CB-RAF600E-1 exerts efficacy in vemurafenib-resistant and non-resistant-melanoma cells via dual inhibition of RAS/RAF/MEK/ERK and PI3K/Akt signaling pathways. Saudi Journal of Biological Sciences. 2022; 29: 103285. https://doi.org/10.1016/j.sjbs.2022.103285.

[25] Al Shahrani M, Abohassan M, Y Alshahrani M, Hakami AR, Rajagopalan P. High-throughput virtual screening and preclinical analysis identifies CB-1, a novel potent dual B-Raf/c-Raf inhibitor, effective against wild and mutant variants of B-Raf expression in colorectal carcinoma. Journal of Computer-aided Molecular Design. 2021; 35: 1165–1176. https://doi.org/10.1007/s10822-021-00426-1.

[26] Swanson K, Walther P, Leitz J, Mukherjee S, Wu JC, Shivnaraine RV, *et al*. ADMET-AI: a machine learning ADMET platform for evaluation of large-scale chemical libraries. Bioinformatics. 2024; 40: btae416. https://doi.org/10.1093/bioinformatics/btae416.

[27] Chen M, Chen X, Chen Q, Chu C, Yang S, Wu C, *et al*. Potential candidates from a functional food *Zanthoxyli Pericarpium* (Sichuan pepper) for the management of hyperuricemia: high-through virtual screening, network pharmacology and dynamics simulations. Frontiers in Endocrinology. 2024; 15: 1436360. https://doi.org/10.3389/fendo.2024.1436360.

[28] Valdés A, Castro-Puyana M, García-Pastor C, Lucio-Cazaña FJ, Marina ML. Time-series proteomic study of the response of HK-2 cells to hyperglycemic, hypoxic diabetic-like milieu. PloS One. 2020; 15: e0235118. https://doi.org/10.1371/journal.pone.0235118.

[29] Welch TR, Frenzke M, Witte D, Davis AE. C5a is important in the tubulointerstitial component of experimental immune complex glomerulonephritis. Clinical and Experimental Immunology. 2002; 130: 43–48. https://doi.org/10.1046/j.1365-2249.2002.01957.x.

[30] 40th International Symposium on Intensive Care & Emergency Medicine: Brussels, Belgium. 24-27 March 2020. Critical Care (London, England). 2020; 24: 87. https://doi.org/10.1186/s13054-020-2772-3.

[31] Peng Q, Wu W, Wu KY, Cao B, Qiang C, Li K, *et al*. The C5a/C5aR1 axis promotes progression of renal tubulointerstitial fibrosis in a mouse model of renal ischemia/reperfusion injury. Kidney International. 2019; 96: 117–128. https://doi.org/10.1016/j.kint.2019.01.039.

[32] Dai ZC, Chen JX, Zou R, Liang XB, Tang JX, Yao CW. Role and mechanisms of SGLT-2 inhibitors in the treatment of diabetic kidney disease. Frontiers in Immunology. 2023; 14: 1213473. https://doi.org/10.3389/fimmu.2023.1213473.

[33] Damm-Ganamet KL, Arora N, Becart S, Edwards JP, Lebsack AD, McAllister HM, *et al*. Accelerating Lead Identification by High Throughput Virtual Screening: Prospective Case Studies from the Pharmaceutical Industry. Journal of Chemical Information and Modeling. 2019; 59: 2046–2062. https://doi.org/10.1021/acs.jcim.8b00941.

[34] Abdul-Hammed M, Adedotun IO, Falade VA, Adepoju AJ, Olasupo SB, Akinboade MW. Target-based drug discovery, ADMET profiling and bioactivity studies of antibiotics as potential inhibitors of SARS-CoV-2 main protease (M^{pro}). Virusdisease. 2021; 32: 642–656. https://doi.org/10.1007/s13337-021-00717-z.

[35] Wennogle LP, Conder L, Winter C, Braunwalder A, Vlattas S, Kramer R, *et al*. Stabilization of C5a receptor–G-protein interactions through ligand binding. Journal of Cellular Biochemistry. 1994; 55: 380–388. https://doi.org/10.1002/jcb.240550316.

[36] Wang N, Zhang C. Oxidative Stress: A Culprit in the Progression of Diabetic Kidney Disease. Antioxidants (Basel, Switzerland). 2024; 13: 455. https://doi.org/10.3390/antiox13040455.

[37] Rieger AM, Nelson KL, Konowalchuk JD, Barreda DR. Modified annexin V/propidium iodide apoptosis assay for accurate assessment of cell death. Journal of Visualized Experiments: JoVE. 2011; 2597. https://doi.org/10.3791/2597.

[38] Luckett-Chastain LR, Gallucci RM. Interleukin (IL)-6 modulates transforming growth factor-beta expression in skin and dermal fibroblasts from IL-6-deficient mice. The British Journal of Dermatology. 2009; 161: 237–248. https://doi.org/10.1111/j.1365-2133.2009.09215.x.

[39] Bosmann M, Haggadone MD, Hemmila MR, Zetoune FS, Sarma JV, Ward PA. Complement activation product C5a is a selective suppressor of TLR4-induced, but not TLR3-induced, production of IL-27(p28) from macrophages. Journal of Immunology (Baltimore, Md.: 1950). 2012; 188: 5086–5093. https://doi.org/10.4049/jimmunol.1102914.

[40] Zheng JM, Zhou HX, Yu HY, Xia YH, Yu QX, Qu HS, *et al*. By Increasing the Expression and Activation of STAT3, Sustained C5a Stimulation Increases the Proliferation, Migration, and Invasion of RCC Cells and Promotes the Growth of Transgrafted Tumors. Cancer Management and Research. 2021; 13: 7607–7621. https://doi.org/10.2147/CMAR.S326352.

[41] Woodruff TM, Nandakumar KS, Tedesco F. Inhibiting the C5-C5a receptor axis. Molecular Immunology. 2011; 48: 1631–1642. https://doi.org/10.1016/j.molimm.2011.04.014.

[42] Lertkiatmongkol P, Liao D, Mei H, Hu Y, Newman PJ. Endothelial functions of platelet/endothelial cell adhesion molecule-1 (CD31). Current Opinion in Hematology. 2016; 23: 253–259. https://doi.org/10.1097/MOH.0000000000000239.

[43] Cao Y, Feng B, Chen S, Chu Y, Chakrabarti S. Mechanisms of endothelial to mesenchymal transition in the retina in diabetes. Investigative Ophthalmology & Visual Science. 2014; 55: 7321–7331. https://doi.org/10.1167/iovs.14-15167.

[44] Li L, Chen L, Zang J, Tang X, Liu Y, Zhang J, *et al*. C3a and C5a receptor antagonists ameliorate endothelial-myofibroblast transition via the Wnt/β-catenin signaling pathway in diabetic kidney disease. Metabolism: Clinical and Experimental. 2015; 64: 597–610. https://doi.org/10.1016/j.metabol.2015.01.014.

[45] Fernández-Hernando C, Suárez Y. MicroRNAs in endothelial cell homeostasis and vascular disease. Current Opinion in Hematology. 2018; 25: 227–236. https://doi.org/10.1097/MOH.0000000000000424.

[46] Stevens T, Garcia JG, Shasby DM, Bhattacharya J, Malik AB. Mechanisms regulating endothelial cell barrier function. American Journal of Physiology. Lung Cellular and Molecular Physiology. 2000; 279: L419–L422. https://doi.org/10.1152/ajplung.2000.279.3.L419.